A multi-channel capacitive probe for electrostatic fluctuation measurement in the Madison Symmetric Torus reversed field pinch

Mingsheng Tan, Douglas R. Stone, Joseph C. Triana, Abdulgader F. Almagri, Gennady Fiksel, Weixing Ding, John S. Sarff, Karsten J. McCollam, Hong Li, and Wandong Liu

Citation: Review of Scientific Instruments **88**, 023502 (2017); doi: 10.1063/1.4975095
View online: http://dx.doi.org/10.1063/1.4975095
View Table of Contents: http://aip.scitation.org/toc/rsi/88/2
Published by the American Institute of Physics

A multi-channel capacitive probe for electrostatic fluctuation measurement in the Madison Symmetric Torus reversed field pinch

Mingsheng Tan,[1] Douglas R. Stone,[2] Joseph C. Triana,[2] Abdulgader F. Almagri,[2,a)] Gennady Fiksel,[3] Weixing Ding,[1,4] John S. Sarff,[2] Karsten J. McCollam,[2] Hong Li,[1] and Wandong Liu[1]

[1]*CAS Key Laboratory of Geospace Environment and Department of Modern Physics, University of Science and Technology of China, Hefei 230026, People's Republic of China*
[2]*Department of Physics, University of Wisconsin, Madison, Wisconsin 53706, USA*
[3]*Center for Ultrafast Optical Sciences, University of Michigan, Ann Arbor, Michigan 48109, USA*
[4]*Department of Physics and Astronomy, University of California, Los Angeles, California 90095, USA*

(Received 18 November 2016; accepted 16 January 2017; published online 8 February 2017)

A 40-channel capacitive probe has been developed to measure the electrostatic fluctuations associated with the tearing modes deep into Madison Symmetric Torus (MST) reversed field pinch plasma. The capacitive probe measures the ac component of the plasma potential via the voltage induced on stainless steel electrodes capacitively coupled with the plasma through a thin annular layer of boron nitride (BN) dielectric (also serves as the particle shield). When bombarded by the plasma electrons, BN provides a sufficiently large secondary electron emission for the induced voltage to be very close to the plasma potential. The probe consists of four stalks each with ten cylindrical capacitors that are radially separated by 1.5 cm. The four stalks are arranged on a 1.3 cm square grid so that at each radial position, there are four electrodes forming a square grid. Every two adjacent radial sets of four electrodes form a cube. The fluctuating electric field can be calculated by the gradient of the plasma potential fluctuations at the eight corners of the cube. The probe can be inserted up to 15 cm ($r/a = 0.7$) into the plasma. The capacitive probe has a frequency bandwidth from 13 Hz to 100 kHz, amplifier-circuit limit, sufficient for studying the tearing modes (5-30 kHz) in the MST reversed-field pinch. *Published by AIP Publishing.* [http://dx.doi.org/10.1063/1.4975095]

I. INTRODUCTION

Electrostatic fluctuations play an important role in the transport of particles[1,2] and energy,[1,2] and the MHD dynamo[3,4] in magnetized plasmas. The mean, equilibrium magnetic field in a reversed field pinch (RFP) plasma has a very strong magnetic shear; the magnetic field is dominantly toroidal in the core, becomes poloidal at the magnetic reversal surface, and develops a small negative component in the toroidal direction in the extreme edge. In the Madison Symmetric Torus (MST),[5] plasma exhibits quasi-periodic impulsive magnetic reconnection events called sawteeth. These sawteeth have a large influence on both plasma fluctuations and mean-field dynamo electromotive force (emf). These reconnection events are driven by several linearly unstable core-resonant tearing modes (with a poloidal mode number $m = 1$ and a broad toroidal mode spectrum $n \geq 6, 7, 8, \ldots$) and serve as the main avenue for magnetic relaxation in RFP plasmas. During this relaxation process, nonlinear interactions energize the linearly stable $m = 0$ modes, resonant at the magnetic reversal surface. These interactions are responsible for the creation of a mean-field dynamo emf that regulates Ohm's law. Generalized Ohm's law includes multiple fluctuation-driven emf terms. The two dominant terms in the RFP plasma are the $\langle \tilde{\mathbf{v}} \times \tilde{\mathbf{B}} \rangle$ known as the MHD dynamo and the $\langle \tilde{\mathbf{J}} \times \tilde{\mathbf{B}} \rangle$ known as the Hall dynamo where $\tilde{\mathbf{v}}$ is the fluctuating velocity, $\tilde{\mathbf{B}}$ is the fluctuating magnetic field, and $\tilde{\mathbf{J}}$ is the fluctuating current density.

Measuring the electrostatic and magnetic fluctuations is critical to the studies of dynamo emf that is responsible for maintaining the RFP state against magnetic diffusion in RFP. Measurement on MST shows that the MHD dynamo and the Hall dynamo emf are what balance Ohm's law in the edge of the MST plasma.[6] Just inside of $r/a = 0.8$, the MHD dynamo was measured to be small and no longer sufficient to balance Ohm's law. However, the Hall dynamo $\langle \tilde{\mathbf{J}} \times \tilde{\mathbf{B}} \rangle$ becomes larger, as the MHD dynamo emf decreases, and sufficient to maintain the balance of Ohm's law.[6,7] The Hall dynamo measurement is extended to $r/a = 0.5$ by using a deep insertion Hall dynamo probe (DIHP).[8] This extended measurement of the Hall dynamo revealed a rich radial structure.

As a result, it would be valuable to extend the electrostatic measurement deeper into the plasma analogous to the deep insertion Hall dynamo probe to investigate the radial structure of the MHD dynamo. However, the standard techniques of measuring electrostatic fluctuations with exposed metal electrodes are limited to the very edge of plasma where the electron temperature is low, few tens of eV. Deeper into the hotter region of the plasma it would be difficult to measure the electrostatic fluctuations. The standard method of measuring electrostatic fluctuation suffers from the metal erosion of the

a)Electronic mail: aalmagri@wisc.edu

electrode that will change the collecting surface area, important for ion saturation measurement, and will also inject high Z impurities into the plasma. In addition, in the triple Langmuir probes configuration, the metal electrodes are in direct contact with the plasma and are biased to few times the local electron temperature. Even though such a probe can measure the plasma potential, the electrodes will arc when the required bias voltage is large.

Single tip Langmuir probes can be made capable of measuring the plasma potential directly by heating the electrode to start emitting electrons so as to reduce the net collected electron current to balance the collected ion current. These are called emissive probes.[9–11] Alternatively, the collected electron and ion currents are balanced by limiting the collected electron current. Such a strategy is incorporated in a Langmuir probe called the "Ball-Pen" probe[12] where the electrode is recessed into a cylindrical shield to reduce the collected electron current. Even though this type of probes measures the plasma potential and requires no bias or heating, it still relies on direct contact with plasma which would limit its application to low temperature plasma.

To overcome the necessity of Langmuir probes to be in direct contact with plasma, a disadvantage, a capacitive probe technique has been introduced. A single tip capacitive probe was designed and constructed to measure the floating potential with a high input impedance, small size, and broad bandwidth by Schmidt.[13] It was formed by a conductor that was separated from the plasma by a glass tube as the dielectric and then capacitively coupled to the plasma. However, such a capacitive probe still measures the floating potential. Boron nitride (BN) ceramics is a better choice of dielectric material due to its high secondary electron emission when bombarded by 18 eV plasma electrons, as shown in Section III. This will create a capacitive probe that is not in direct contact with the plasma and measures the plasma potential.[14] Such a probe design eliminates the two shortcomings of a standard Langmuir probe.

The probe described here employs BN as the dielectric. A BN shielded capacitive probe can then measure the plasma potential directly and will not be limited to the extreme plasma edge. The BN also serves as the plasma facing material and it can survive in about 100 eV plasma. As the plasma facing material, BN is made to emit secondary electrons by the plasma itself. A capacitive probe that measures the plasma potential at spatial points that are separated toroidally, poloidally, and radially can be used to measure the electric field fluctuations by the gradient of the plasma potential fluctuations $\tilde{\mathbf{E}}_s = -\nabla \tilde{V}_p$, where $\mathbf{E}_s$ is the electric field and V_p is the plasma potential.

A probe that is capable of measuring the vector electric field at a single radial location in the edge of MST was built and has shown the compatibility of such a probe with the MST plasma. A probe that is capable of measuring the vector electric field inside of $r/a = 0.9$ would provide previously unavailable information about the MHD dynamo profile, and radial correlation lengths of electrostatic fluctuations, to compliment the interesting radial structure of the Hall dynamo measured on MST. The multiple stalks' design is also capable of measuring the wavenumber power spectral density of the electric field fluctuations. The probe described in this paper has been designed, built, and tested in the MST plasma but initially limited to $r/a \geq 0.7$.

MST[5] is a large RFP with a major radius $R = 1.5$ m, a minor radius $a = 0.52$ m, plasma current $I_p \leq 600$ kA, electron density $n_e \approx 0.3 - 3 \times 10^{19}$ m^{-3}, electron temperature $T_e \sim 600$ eV, and a discharge duration of 60-80 ms. However, the experiments described in this article are done at much reduced plasma parameters due to BN limitations. These plasma parameters are 200 kA or less for plasma current, electron density of $n_e \approx 1 \times 10^{19}$ m^{-3}, and on axis electron temperature $T_e < 200$ eV. This is done to minimize erosion to the BN surface. This is important for two reasons. First, the probe calibration is impacted by the reduced thickness of the BN dielectric. Second, erosion of BN is an important source of boron and nitrogen impurities' injection into the plasma.

This paper is organized as follows: Section II will describe the details of the capacitive probe design. Section III will describe the secondary electron emission properties of the BN particle shield. Circuit gain and calibration will be presented in Section IV. Finally, initial measurements are presented in Section V.

II. THE 40-CHANNEL CAPACITIVE PROBE DESIGN

This probe is capable of measuring plasma potential fluctuations at 40 different spatial locations. The probe consists of four stalks. Each stalk contains ten 1.0 cm long cylindrical capacitors with 1.5 cm axial separation. For the ease of identification, the four stalks are labeled as A, B, C, and D and the capacitors are labeled as A1:A10, B1:B10, C1:C10, and D1:D10. When inserted into the plasma, the probe will measure the ac component of the plasma potential at four locations on a 1.3 cm square grid at each of the 10 radial locations. When differencing the potential measurement, the probe can measure the electric field along the four sides of the square grid. Each two of the four electric field measurements are of the same field component but separated by 1.3 cm toroidally or poloidally. Using the two-point spectrum method, the wavenumber spectrum of the measured potential and electric field fluctuations can be calculated. The probe is also instrumented with two magnetic pickup coils that are used for probe alignment. The probe can be aligned into two configurations as shown in Fig. 3. The first configuration is when the sides of the square grid are in the toroidal and poloidal directions. The second configuration is when the diagonals of the square grid are aligned in the toroidal and poloidal directions.

The layout of the probe without the BN particle shields, the dielectric, exposing the cylindrical capacitors is shown in Fig. 1. It consists of four supporting stalks made of BN, which have an axial trench to house the ten miniature coaxial cables. The central conductor of each coaxial cable is connected to its respective stainless steel cylindrical electrode. The shield of the coaxial cable serves as an electrostatic shield of the signal. The cylindrical electrodes fit tightly over the supporting stalks and are separated by 0.5 cm BN spacers to maintain 1.5 cm electrode radial separation. The overall BN sleeve is

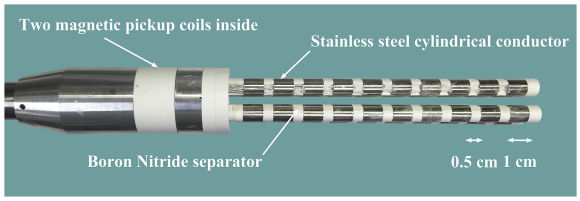

FIG. 1. Photograph of the 40-channel capacitive probe without the BN particle shields.

shown in Fig. 2. It serves multiple functions. First, it is the particle shield that separates the plasma from the electrodes, in order to protect the metal electrodes from plasma energetic particles and eliminate electrode sputtering. Second, the sleeve serves as the capacitor dielectric between the plasma and the electrode. BN is a good choice for the sleeve material for two reasons. First, it can survive a 100 eV, high density, and low current plasma with very little erosion. Second, and more important, it has a high secondary electron emission. As a result, the probe sleeves are designed to be replaced with ease before erosions of BN become significant and impact the probe calibration.

Two perpendicular magnetic pickup coils are utilized for the probe alignment. The two magnetic pickup coils are wound on the BN bobbin and housed in the BN particle shield at the base of the four stalks to prevent plasma damage to the magnet wire, see Fig. 1. The signals of the pickup coils are integrated. The pickup coils are at the base of two stalks as shown in Fig. 3. One coil axis is aligned along the D → B direction and the other pickup coil axis is aligned along the A → C direction. MST can operate in a vacuum-shot mode where the toroidal magnetic field is large, up to 500 gauss, and zero poloidal magnetic field with no plasma. With vacuum shots, the probe can be rotated until the pickup coil at the base of stalk B is zeroed as shown in Fig. 3. At this point, the probe is in configuration (b), the "diamond" arrangement. Alternatively, the pickup coil at the base of stalk A can be zeroed which also would produce configuration (b) since all four stalks are identical. Configuration (a), the "square" arrangement can be achieved by rotating the probe an additional 45° using the integrated protractor with 0.1° accuracy.

The first configuration allows for the measurement of the electric field at two points that are poloidally and toroidally separated to enable two-point wavenumber spectrum measurement. The second configuration allows for a single point measurement of the poloidal and toroidal electric fields at the center of the diamond.

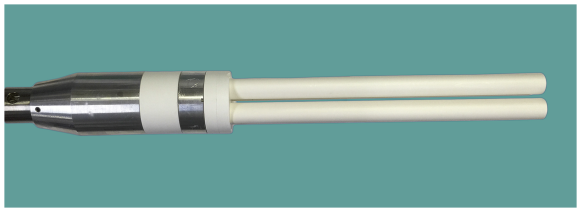

FIG. 2. Photograph of the completely assembled 40-channel capacitive probe.

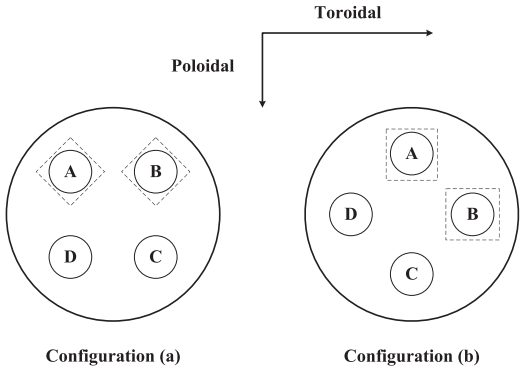

FIG. 3. Two configurations of the probe geometry: A, B, C, and D are the labels of the four stalks and the two dashed squares represent the two magnetic pickup coils.

III. SECONDARY ELECTRON EMISSION

When a material probe is inserted into plasma, it will experience collisions with the plasma electrons and ions. Since ions are typically massive and less mobile than electrons, the electrons dominate in colliding with the probe. Some of the incoming plasma electrons will scatter off the probe and the majority will collide and form a sheath surrounding the electrode. As a result, the probe voltage is at the floating potential. In addition to the scattered plasma electrons, some electrons from the probe material will be released after absorbing energy from the incoming plasma electrons. The incoming plasma electrons that collide with the electrode are called the "primary" electrons. Electrons coming off the probe can be sorted into two groups. The first group is the plasma electrons that scattered off the electrode. The second group is the electrons that are liberated from the probe material due to a collision of the incoming plasma electron with the probe; these are called the "secondary" electrons. The number of the secondary electrons liberated for a given primary electron at an energy E_p depends on the type of the probe material. For a material with a low secondary electron emission, the electron current to the probe is much larger than the ion current to the probe. Such a probe will be at the floating potential due to the formation of sheath. However, for a material with a high secondary electron emission, the electron current to the probe is balanced with the ion current. Such a probe will be at the plasma potential.

BN emits a large secondary electron emission current when bombarded with energetic plasma electrons. The secondary electron emission (SEE) current yield, $\sigma\left(E_p\right)$, is the ratio of secondary electrons to primary electrons, where E_p is the colliding primary electron energy. The floating potential measured by the probe in the presence of secondary electron emission can be expressed as[15]

$$V_f = V_p - \frac{kT_e}{e} \ln\left(\frac{1-\sigma\left(T_e\right)}{\sqrt{2\pi m_e/m_i}}\right), \tag{1}$$

where V_p is the plasma potential, T_e is the electron temperature, m_e is the electron mass, and m_i is the ion mass. $\sigma\left(T_e\right)$ is the SEE total yield integrated over the electron distribution function.

The total current yield of SEE, $\sigma(E_p)$, was measured for BN from Saint Gobain Corp. Using a power law, $\sigma(E_p)$ can

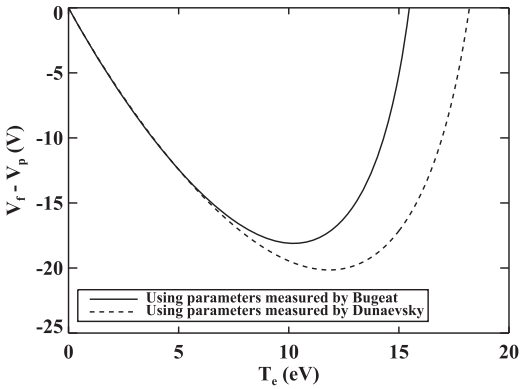

FIG. 4. Probe floating potential relative to the plasma potential for a thermal electron distribution, using parameters reported by Bugeat and Dunaevsky.

be fit as $\sigma(E_p) = (E_p/E_1)^{\alpha}$. Integrating this SEE current yield over a thermal electron distribution gives[16]

$$\langle \sigma(T_e) \rangle = \left(\frac{\langle E_p \rangle}{2E_1} \right)^{\alpha} \Gamma(2+\alpha), \tag{2}$$

where $\langle E_p \rangle = 2kT_e$ is the average primary electron energy.

For a BN material of HP grade, used in MST, Bugeat[17] gives $E_1 \approx 30$ eV and $\alpha = 0.57$, and Dunaevsky[16] gives $E_1 \approx 35$ eV and $\alpha = 0.5$. Using Eqs. (1) and (2), a plot of $(V_f - V_p)$ versus T_e is shown in Fig. 4 for the two models. For a cold plasma ($T_e = 0$ eV), the electrons are stationary like the ions resulting in low and identical electrons and ion currents, and the probe is at the plasma potential. As the plasma gets hotter, the electrons become more mobile and an imbalance of electron and ion currents occurs due to insufficient SEE. As the electron energy increases, the SEE increases resulting in a reduced difference between V_f and V_p. The maximum of $(V_f - V_p)$ occurs at $T_e = 10$ eV for BN parameters. As the electron temperature increases further, the SEE increases to the point where V_f is nearly equal to V_p; this occurs at $T_e = 18$ eV for BN parameters. Both models, using BN parameters, show that the floating potential approaches the plasma potential value as the plasma electron temperature approaches 18 eV. When the plasma temperature is larger than 18 eV, the floating potential should be equal to the plasma potential because secondary electrons are of low energy and would be reabsorbed when $V_f > V_p$.

IV. CIRCUIT GAIN AMPLITUDE AND PHASE CALIBRATION

Plasma potentials are typically in the hundreds of volts. To measure these high potentials, a capacitive divider circuit is required. The capacitor formed by the plasma and the electrode is called the "coupling" capacitor. This "coupling" capacitor is connected to a capacitive divider circuit, see Ref. 13, to attenuate the probe voltage output before it is sent via an operational amplifier to a digitizer, see Fig. 5. The large resistance R sets the low cutoff frequency of the circuit. Capacitance C_1 is the coupling capacitance, C_2 is the capacitance of the coaxial cable, and C_3 is the capacitor of the capacitive divider circuit. Parameters used for this probe are as follows. The coupling capacitance $C_1 \sim 7$ pF estimated from the circuit gain,

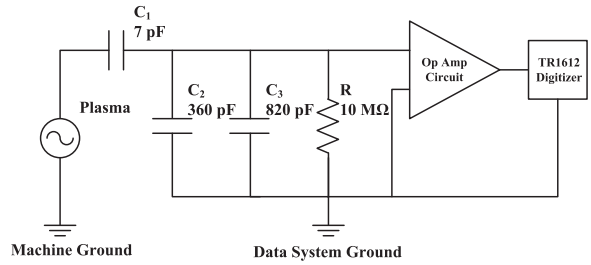

FIG. 5. The capacitive probe circuit.

$C_2 \sim 360$ pF estimated from cable lengths, $C_3 \sim 820$ pF, and R = 10 mΩ. C_1 can be estimated by the following formula:

$$C_1 = \frac{2\pi l}{\ln(r_2/r_1)/\varepsilon_0 + \ln(r_3/r_2)/\varepsilon}, \tag{3}$$

where l is the length of the conductor, ε_0 is the permittivity of vacuum, ε is the permittivity of BN, r_1 is the outer radius of conductor, and r_2 and r_3 are the inner and outer radii of BN dielectric, respectively.

From the capacitor-geometric values and choosing $\varepsilon_{BN} = 3\varepsilon_0$, the coupling capacitor is $C_1 = 6.88$ pF. The circuit attenuation is equal to $C_1/(C_1 + C_2 + C_3) \sim 0.006$ which is sufficient to reduce the plasma potential from hundreds of volts to few volts before digitization. The operational amplifier isolates the probe/circuit from the digitizer. This amplifier has a constant unity gain at low frequencies and rolls off at high frequencies with a 3 dB point at 100 kHz. The upper-frequency limit is set by the amplifier. The lower-frequency limit is set by the capacitive divider circuit given by $f_{low} = 1/[2\pi R(C_2 + C_3)] \sim 13$ Hz. The overall frequency response of the circuitry is 13 Hz $< f <$ 100 kHz. The digitizer is set to 500 kHz sampling frequency which is sufficient to measure the tearing modes fluctuation (5-20 kHz) of interest in MST and double the upper frequency limit to prevent signal aliasing.

For the case of a single stalk probe, it would be easy to insert the probe into a conducting block with close fitting hole to do the calibration, as was done in Ref. 13. However, for the four stalk probes, it is more convenient to spray the four particle shields with dry graphite, which will surround the probe with a continuous, no air gap coating to simulate the plasma. The thickness of the graphite layer is in sub millimeters and is hard to measure precisely. However, only a thin layer of graphite is required. It is important for the BN surface to be very smooth and free of debris before applying the graphite.

A soft conducting copper braid is used to connect the signal generator to the graphite. The copper braid is tightly twisted on the graphite. Due to the very low current in the braid, there is no voltage drop across the braid or the contact joint with graphite. When the calibration is complete, the graphite layer is removed so as not to introduce graphite into the plasma but more importantly the plasma must be on the other side of the capacitor. The circuit gain is measured by applying a sinusoidal voltage, from a signal generator, to the graphite. The generator signal frequency is varied from 10 Hz up to 150 kHz. The generator signal, input, and the

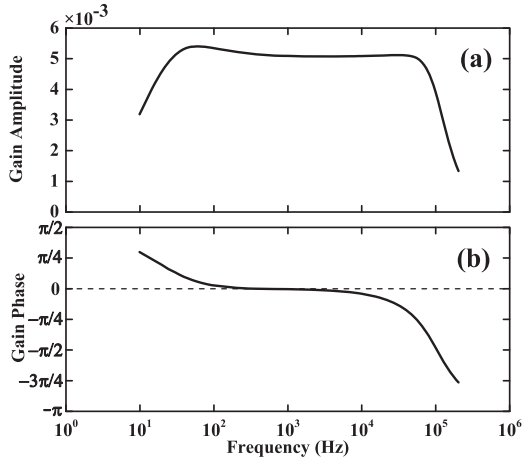

FIG. 6. An example of the circuit gains' calibration of the capacitive probe: (a) gain amplitude; (b) gain phase.

probe's 40 capacitor signals, output, are digitized simultaneously for each frequency. The data are transformed from the time to frequency domain by the Fast Fourier Transform (FFT) algorithm. The complex gain is formed by the ratio of the output probe signals to the generator signal at each frequency.

Fig. 6 is an example of the circuit complex gain, amplitude, and phase. The measured gain is very similar to the expected capacitor divider value. The figure shows only the gain of the positive frequencies; the gains of the negative frequencies are the conjugate of the gains of the positive frequencies ($G(-f) = G^*(f)$). The probe is calibrated before it is inserted into the plasma. The particle shields were replaced after about 300 discharges, to minimize changes in the circuit gains resulting from the reduced particle shield thickness, due to the plasma sputtering, which would change the capacitance of the coupling capacitor.

V. INITIAL MEASUREMENTS

The results described here are from experiments carried out in MST with a plasma current $I_p = 200$ kA, line-averaged electron density $\bar{n}_e = 1.0 \times 10^{19}$ m^{-3}, reversal parameter F (toroidal field at the wall/average toroidal field) = −0.2, and pinch parameter Θ (poloidal field at the wall/average toroidal field) = 1.7. At low current and high plasma density, it is possible to routinely operate the capacitive probe in the outer 15 cm of the plasma ($0.7 \le r/a \le 1$) with low erosion of the particle shield. Data from stalk C will be used in this section to demonstrate the measurements made by the capacitive probe. The other three stalks, A, B, and D are used to determine the three components of the electric field and their radial profiles (which are not shown in this article). An example of the raw signal of the capacitive probe (capacitive probe labeled as C1) at $r/a = 0.7$ is shown in Fig. 7. The plasma potential is obtained by dividing the raw signals of the probe by the complex gains $G(f)$ in the frequency domain. The resulting plasma potential is shown in Fig. 8.

MST plasmas exhibit quasi-periodic magnetic reconnection events known as sawtooth crashes with a period of a few milliseconds. Fig. 9 is the time traces of the plasma current and

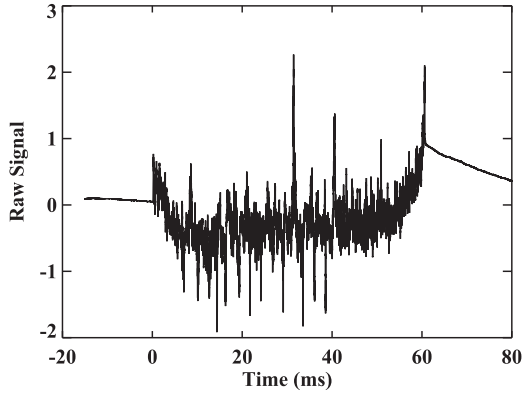

FIG. 7. An example of the raw signal of the capacitive probe (the capacitive probe C1).

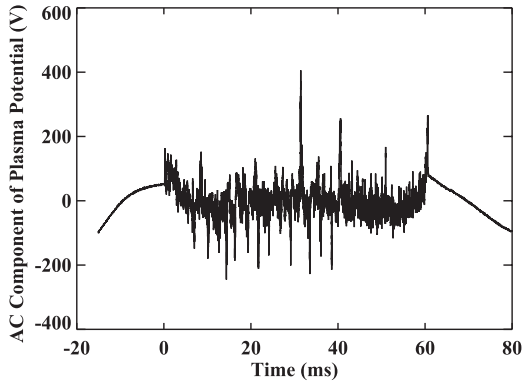

FIG. 8. The ac component of the plasma potential measured by the capacitive probe C1.

cross section-averaged toroidal magnetic field where the times of sawtooth crash events during the flat-top phase are shown. These events are driven by the nonlinear coupling of the linearly unstable core resonant tearing modes ($m = 1$, $n \ge 5$), as they destabilize edge resonant modes ($m = 0$, $n = 1, 2, 3$). Conditional sawtooth averaging of the plasma potential signal, a standard technique on MST, is used to study the variation of the fluctuations in amplitude and phase versus time relative to sawtooth crash. For each sawtooth crash, the time of maximum change of the cross section-averaged toroidal magnetic field is redefined to be zero time. Data within a time window that is 2 ms wide and centered on the time of crash, $t = 0$, are

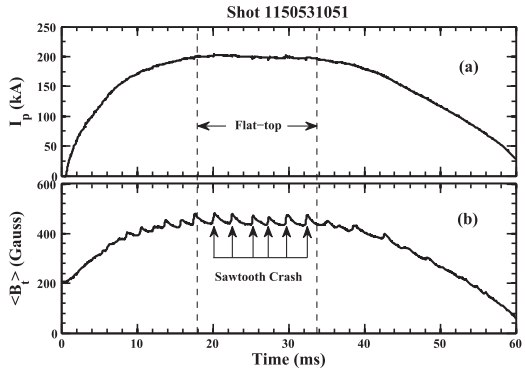

FIG. 9. Time traces of (a) plasma current and (b) cross section-averaged toroidal magnetic field. Times of sawtooth crash events during the flat-top phase are shown.

treated as one sawtooth event. All sawtooth events that satisfy the following conditions are included in the ensemble; the sawtooth must occur during the flat top of the discharge and when the plasma current, density, and reversal parameter, are within a pre-specified narrow range. Typically, there are many hundreds of these events that are averaged to get the equilibrium value. This technique of conditional sawtooth averaging is considered to be a proxy for the flux surface average under two conditions. First, the plasma is rotating toroidally. Second, the phase of the sawtooth is random, so-called the random phase approximation. When these two conditions are satisfied, then the average of many single-point measurements is equivalent to a flux surface average of that quantity. Fig. 10 shows the equilibrium plasma potential profile measured by the capacitor C1 ($r/a = 0.8$) through C7 ($r/a = 0.97$). In the outer 10 cm of the MST edge plasma ($r/a \geq 0.8$), the potential profile is flat and near zero volts before a sawtooth crash. The potential becomes negative during the sawtooth crash, reaching −50 V at the crash, and more negative from the edge inward, consistent with high electron transport at the sawtooth crash. At the sawtooth crash, magnetic stochastic transport is enhanced resulting in increased electron loss from the core towards the edge. The extreme edge of the plasma is limited by a grounded limiter, zero potential. Away from the limiter, there is an abundance of electrons at the time of sawtooth crash. This potential profile results in an inward pointing radial electric field. After the sawtooth crash, the potential relaxes as electrons are lost to the wall. While the limiter is still pinned at zero volt; the potential, inside the limiter, is positive resulting in an outward pointing radial electric field. As shown in Fig. 10, the potential becomes positive and increasingly more positive away from the edge after the crash. The potential peaks to +30 V at 0.5 ms after the crash. The edge profile is then restored to flat. The plasma potential at $r/a \sim 0.4$ was measured by the Heavy Ion Beam Probe (HIBP).[18] The measured radial electric field was found to be consistent with $\mathbf{E} \times \mathbf{B}$ plasma flow.

The fluctuation component of the signal is obtained by subtracting the equilibrium, sawtooth average, obtained earlier from the total signal for each sawtooth crash. The root mean square (RMS) values of the plasma potential fluctuation profile measured by stalk C are shown in Fig. 11. At 1 ms before the crash, the RMS value of $\tilde{V}_p$ increases from about 10 V at

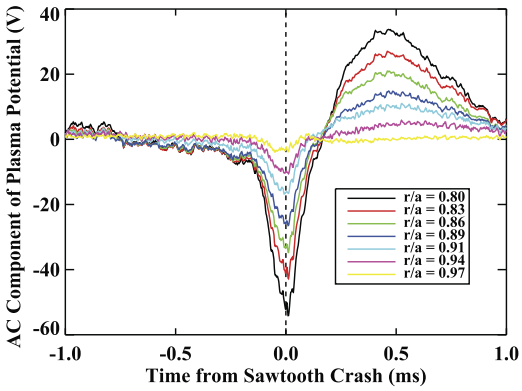

FIG. 10. Equilibrium plasma potential profile measured by stalk C of the 40-channel capacitive probe.

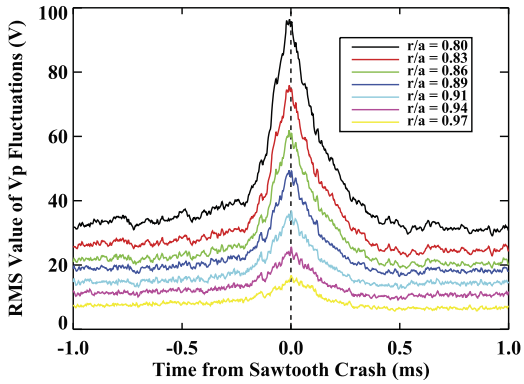

FIG. 11. The root mean square of the plasma potential fluctuation profile measured by stalk C of the 40-channel capacitive probe.

$r/a = 0.97$ up to about 35 V at $r/a = 0.8$. During the sawtooth crash, the RMS burst to near 100 V at $r/a = 0.8$ while the edge value, $r/a = 0.97$, only increases to about 15 V. From all four stalks on the capacitive probe, the electrostatic field can be obtained. Such data can be combined with magnetic field measurements to obtain fluctuating flow velocities using $\mathbf{E} \times \mathbf{B}$.

SUPPLEMENTARY MATERIAL

See supplementary material for the digital format of the data shown in this paper.

ACKNOWLEDGMENTS

This research was supported by the U.S. Department of Energy, Office of Science, Office of Fusion Energy Sciences program under Award No. DE-FC02-05ER54814. M. Tan was supported by the National Magnetic Confinement Fusion Energy Program of China under Contract No. 2011GB106000.

[1]T. D. Rempel, C. W. Spragins, S. C. Prager, S. Assadi, D. J. D. Hartog, and S. Hokin, Phys. Rev. Lett. **67**, 1438 (1991).
[2]T. D. Rempel, A. F. Almagri, S. Assadi, D. J. D. Hartog, S. A. Hokin, S. C. Prager, J. S. Sarff, W. Shen, K. L. Sidikman, C. W. Spragins, J. C. Sprott, M. R. Stoneking, and E. J. Zita, Phys. Fluids B **4**, 2136 (1992).
[3]H. Ji, A. F. Almagri, S. C. Prager, and J. S. Sarff, Phys. Rev. Lett. **73**, 668 (1994).
[4]H. Ji, S. C. Prager, A. F. Almagri, J. S. Sarff, Y. Yagi, Y. Hirano, K. Hattori, and H. Toyama, Phys. Plasmas **3**, 1935 (1996).
[5]R. N. Dexter, D. W. Kerst, T. W. Lovell, S. C. Prager, and J. C. Sprott, Fusion Technol. **19**, 131 (1991).
[6]A. Kuritsyn, G. Fiksel, A. F. Almagri, D. L. Brower, W. X. Ding, M. C. Miller, V. V. Mirnov, S. C. Prager, and J. S. Sarff, Phys. Plasmas **16**, 055903 (2009).
[7]T. D. Tharp, A. F. Almagri, M. C. Miller, V. V. Mirnov, S. C. Prager, J. S. Sarff, and C. C. Kim, Phys. Plasmas **17**, 120701 (2010).
[8]J. C. Triana, A. F. Almagri, K. J. McCollam, J. S. Sarff, J. P. Sauppe, and C. R. Sovinec, *The Exploratory Plasma and Fusion Research Workshop* (Auburn, Alabama, 2016).
[9]I. Langmuir, J. Franklin Inst. **196**, 751 (1923).
[10]J. P. Sheehan, Y. Raitses, N. Hershkowitz, I. Kaganovich, and N. J. Fisch, Phys. Plasmas **18**, 073501 (2011).
[11]J. P. Sheehan and N. Hershkowitz, Plasma Sources Sci. Technol. **20**, 063001 (2011).
[12]J. Adámek, J. Stöckel, M. Hron, J. Ryszawy, M. Tichý, R. Schrittwieser, C. Ionită, P. Balan, E. Martines, and G. V. Oost, Czech. J. Phys. **54**, C95 (2004).

[13]J. A. Schmidt, Rev. Sci. Instrum. **39**, 1297 (1968).
[14]D. R. Stone, "Magnetic relaxation during oscillating field current drive in a reversed field pinch," Ph.D. thesis, University of Wisconsin, Madison, 2013.
[15]G. D. Hobbs and J. A. Wesson, Plasma Phys. **9**, 85 (1967).
[16]A. Dunaevsky, Y. Raitses, and N. J. Fisch, Phys. Plasmas **10**, 2574 (2003).
[17]J. P. Bugeat and C. Koppel, in *Proceedings 24th International Electric Propulsion Conference* (The Electric Rocket Propulsion Society, Worthington, OH, Moscow, Russia, 1995).
[18]D. R. Demers, J. Lei, U. Shah, P. M. Schoch, K. A. Connor, T. P. Crowley, and J. G. Schatz, in *28th EPS Conference on Contribution Fusion and Plasma Physics* (CRPP, Centre de recherches en physique des plasmas. Ecole polytechnique fédérale, 2001), Vol. 25A, pp. 161–164.